Nuclear Science and Techniques (2024) 35:75
https://doi.org/10.1007/s41365-024-01436-y

Beam based alignment using a neural network

Guan-Liang Wang[1] · Ke-Min Chen[1] · Si-Wei Wang[2] · Zhe Wang[1] · Tao He[1] · Masahito Hosaka[1] · Guang-Yao Feng[1] · Wei Xu[1]

Received: 28 September 2023 / Revised: 7 December 2023 / Accepted: 21 December 2023 / Published online: 24 May 2024

Abstract
Beams typically do not travel through the magnet centers because of errors in storage rings. The beam deviating from the quadrupole centers is affected by additional dipole fields due to magnetic field feed-down. Beam-based alignment (BBA) is often performed to determine a golden orbit where the beam circulates around the quadrupole center axes. For storage rings with many quadrupoles, the conventional BBA procedure is time-consuming, particularly in the commissioning phase, because of the necessary iterative process. In addition, the conventional BBA method can be affected by strong coupling and the nonlinearity of the storage ring optics. In this study, a novel method based on a neural network was proposed to determine the golden orbit in a much shorter time with reasonable accuracy. This golden orbit can be used directly for operation or adopted as a starting point for conventional BBA. The method was demonstrated in the HLS-II storage ring for the first time through simulations and online experiments. The results of the experiments showed that the golden orbit obtained using this new method was consistent with that obtained using the conventional BBA. The development of this new method and the corresponding experiments are reported in this paper.

Keywords Golden orbit · Beam-based alignment · Neural network · Storage ring

1 Introduction

Ideally, the beam in a storage ring should circulate on the orbit passing through the axes of all magnet centers, which is called the golden orbit. The beam orbit may deviate from the ideal path due to errors such as misalignment, magnet imperfection, and power regulation errors. When the beam traverses magnets with orbital offsets, undesired magnetic fields are observed, called feed-downs [1]. The feed-down of a quadrupole with an orbital offset causes an additional dipole field. To minimize this effect, a beam-based alignment can be adopted to determine the golden orbit for machine operation. It is widely used in the commissioning phase of storage rings [2, 3]. For storage rings with long circumferences, such as most diffraction-limited storage rings (DLSRs), the number of quadrupoles is large, and the conventional BBA method is time-consuming [4]. Recently, a fast BBA method was developed at ALBA light source using the AC excitation of orbit correctors and fast beam position data acquisition [5–7]. At HLS-II, with no need to upgrade the hardware, a machine learning (ML)-based method was developed to determine the golden orbit for storage rings [8].

Neural networks (NNs) have been widely applied in artificial intelligence and have achieved great success in various fields. Their application has also been introduced in the field of particle accelerators [9–12]. In the Advanced Light Source (ALS), an NN model is used to maintain the vertical beam size when the gap of insertion devices varies [13]. The NN model can also be used to significantly reduce the simulation time for beam dynamics optimization [14]. At the Shanghai Synchrotron Radiation Facility (SSRF), an image processing technique using convolutional neural networks (CNNs) was adopted to extract bunch longitudinal phase information [15]. These applications demonstrate the substantial potential of NNs for improving accelerator performance.

This work was supported by the National Natural Science Foundation of China (No. 11975227).

✉ Wei Xu
wxu@ustc.edu.cn

1 National Synchrotron Radiation Laboratory, University of Science and Technology of China, Hefei 230029, China

2 Diamond Light Source, Oxfordshire OX11 0DE, UK

In this study, we present a new BBA method that uses an NN model to predict the golden orbit of a storage ring. To initiate the experiment, different closed orbits were generated by randomly changing the strengths of all the orbit correctors. Beams with various orbital deviations in the quadrupoles are subject to various degrees of influence from their magnetic field feed-down. This effect can be evaluated by measuring the change in the orbit caused by the quadrupole strength variation. Because the beam on the ideal golden orbit should not be disturbed by changing the quadrupole strength, an NN model can be trained to search for the orbit that is least affected by varying the quadrupole strength. To train this model, the orbit differences owing to quadrupole changes were used as input data, and the corresponding orbits before quadrupole adjustment were used as output data. The golden orbit was predicted by setting the input value to zero in the NN model.

To demonstrate its validity, the new BBA method was tested in the HLS-II storage ring through simulations and online experiments. The results indicated that the golden orbit obtained from the NN model was consistent with that obtained after several iterations using the conventional method. The golden orbit obtained using this method can be directly used for operation or as a starting point to speed up the conventional BBA, which requires several iterations. In general, this new method is less time-consuming than the conventional BBA, particularly during initial commissioning [16].

In the following sections, the methods of the conventional BBA and the new BBA using an NN model are shown in Sect. 2. The simulation results obtained using these two BBA methods for the HLS-II storage ring are described in Sect. 3. The online experiments using both BBA methods are introduced in Sect. 4. Finally, the work is summarized in Sect. 5.

2 Beam-based alignment

2.1 Conventional BBA method

The purpose of BBA is to find a reference orbit in which the beam passes the centers of all quadrupoles in a storage ring using beam position monitors (BPMs) and orbit corrector magnets (OCMs). The dipole fields seen by an off-axis particle in a quadrupole is given by

$$B_x = B_0\rho_0 K_0 y_0, \tag{1}$$

$$B_y = B_0\rho_0 K_0 x_0, \tag{2}$$

where $B_0\rho_0$ is the magnetic rigidity, K_0 is the normalized quadrupole strength, and x_0 and y_0 are the beam offsets relative to the quadrupole center in the horizontal and vertical planes, respectively. Therefore, changing the quadrupole strength by ΔK causes a dipole field variation by

$$\Delta B_x = B_0\rho_0 \Delta K y_0, \tag{3}$$

$$\Delta B_y = B_0\rho_0 \Delta K x_0, \tag{4}$$

resulting in a kick that leads to an orbital change at the observation point s by [17]

$$\begin{aligned}\Delta \boldsymbol{u}(s) =& \Delta K \boldsymbol{u}(s_0)\left(\frac{1}{1-K_0\frac{L_0\beta(s_0)}{2\tan(\pi\nu)}}\right)\\ &\times\frac{\sqrt{\beta(s)\beta(s_0)}}{2\sin(\pi\nu)}\cos(|\phi(s)-\phi(s_0)|-\pi\nu),\end{aligned} \tag{5}$$

where L_0 is the length of the quadrupole, ν is the betatron tune, and $\beta(s_0)$ and $\beta(s)$ are the beta functions at the locations of the quadrupole and observation points, respectively. $\phi(s_0)$ and $\phi(s)$ are the phase advances at the locations of the quadrupole and observation points, respectively, and $\boldsymbol{u}$ represents the beam positions in the horizontal and vertical planes. This equation shows that the beam orbit can be affected by the quadrupole strength variation and beam positions in the quadrupoles. To avoid this effect, the reference orbit of the orbit feedback system is typically set to the centers of all quadrupoles with $\boldsymbol{u} = \boldsymbol{0}$. The reference orbit is determined using the BBA technique.

The quadrupole center is measured using the nearest BPM. Suppose that when the beam passes through the quadrupole center, the related reading of this BPM is $\boldsymbol{v}_0$. According to Eq. (5), by changing the quadrupole strength ΔK, the beam orbit change is given by

$$\Delta \boldsymbol{u} = \Delta K \mathcal{F}(\boldsymbol{v}-\boldsymbol{v}_0), \tag{6}$$

where $\boldsymbol{v}$ is the reading of the target BPM before the quadrupole strength change, and $\mathcal{F}$ is the coefficient that can be easily obtained from Eq. (5). To measure the quadrupole center, the beam is set to several different positions at its related BPM. For each position, the quadrupole strength is varied with the same ΔK, and the corresponding orbit changes are recorded. By applying a linear fit to Eq. (6), the quadrupole center $\boldsymbol{v}_0$ is obtained. The conventional BBA always determines the horizontal and vertical offsets separately [18]. The above analysis implies that the coefficient $\mathcal{F}$ is treated as a constant, which implies that the beam optics remain unchanged during the BBA process. In fact, the change in quadrupole strength and closed orbit distortion can affect the beam optics. At the beginning of commissioning, the beam orbit and beam optics are possibly significantly different from the ideal model, which induces strong nonlinearity and coupling. In this case, several iterations are required for the conventional BBA method to eliminate the nonlinear effects and obtain more accurate quadrupole centers. A neural network with multiple layers that address nonlinear problems can be adopted for the BBA process [19, 20].

2.2 BBA using a neural network

BBA is based on the principle that the off-axis beam is affected by a quadrupole strength change. The golden orbit can then be evaluated using the relationship between the orbit changes and the initial beam orbits before varying the quadrupole strength. This relationship can be explored by training a neural network using orbital changes as the input data and initial orbits as the output data. By setting the orbital change to zero, the corresponding initial beam orbit becomes the predicted golden orbit. The main concept behind this proposed BBA method is illustrated in Fig. 1. To obtain data for training the NN model, a simulation or online experiment was performed as follows:

- Randomly exciting all corrector magnets to form an initial closed orbit;
- recording all BPM readings;
- changing all quadrupoles by the same amount to form a new closed orbit.
- recording the changes in all BPM readings;
- resuming the quadrupole and corrector strengths to the original values;
- repeating the above procedures.

A typical dense neural network has one input layer, several hidden layers (also called middle layers), and one output layer, as illustrated in Fig. 2 [21]. The nodes where the data are transferred are called neurons. The nodes between adjacent layers are connected to each other by an arrow, which shows the flow of data. Each arrow represents a linear transformation combined with an activation function used to introduce nonlinearity if necessary [11]. A loss function is used to describe the performance of the neural network. An NN also requires an optimizer function to optimize the parameters used for data transmission. The optimization is performed by minimizing the loss value.

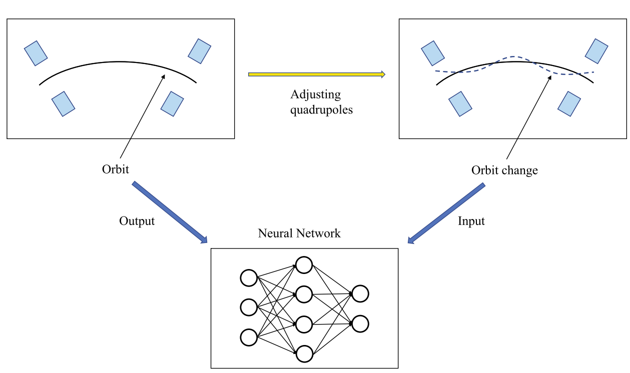

Fig. 1 Schematic of the neural network-based BBA method. Different orbits are generated by randomly adjusting the orbit correctors. On each orbit, all quadrupoles are changed with the same ΔK simultaneously to generate orbit changes. The orbit changes are used as the input data of the neural network, and the corresponding initial orbits are used as the output data for the training

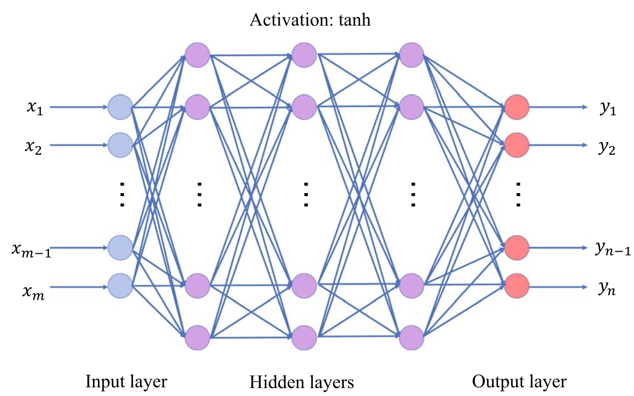

Fig. 2 Diagram of a typical dense neural network, which consists of one input layer, several hidden layers, and one output layer. Here, the hyperbolic tangent (tanh) is adopted as the activation function

3 Simulation study for the HLS-II storage ring

Before conducting the online experiments, a simulation was performed to evaluate the validity of the new BBA method based on an NN model. The accelerator toolbox (AT) is used for the simulation in this study [22]. TensorFlow, which is adopted in this study, provides a flexible platform that makes it easy for users to build and train an NN model [23, 24].

The HLS-II storage ring has two super periods with a circumference of 66.1m. The layout of a single super period is shown in Fig. 3. The orbit system of the storage ring consists of 32 BPMs and 32 correctors combined with sextupoles. 32 quadrupoles were installed to measure their real centers using the BBA procedure [25].

Random rotation and shift errors were applied to simulate the misalignment of the elements and girders. The errors were generated in a normal distribution with truncation at three standard deviations. Based on the design report, the error settings for all magnets, girders, and BPMs are listed in Table 1. A set of misalignment errors for the whole ring is shown in Table 4. Strength errors of all magnets were also applied. The BPM random measurement error was set to 0.5 μm [26].

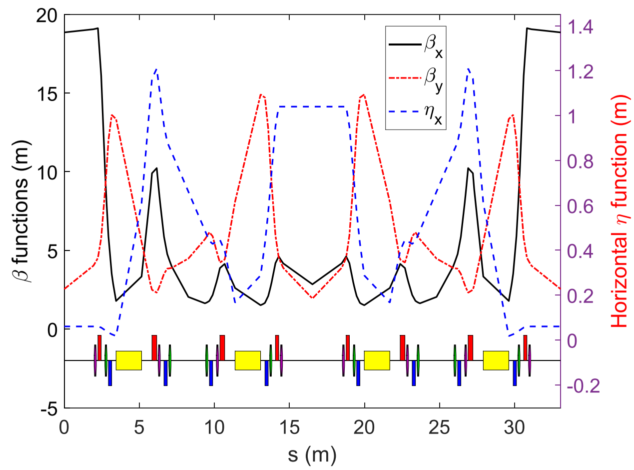

Fig. 3 One super period of the HLS-II lattice. There are 32 quadrupoles and 32 BPMs in the storage ring. The 32 combined-function sextupoles are used as the horizontal and vertical correctors

3.1 Conventional BBA method

In the conventional BBA measurement for one quadrupole, the beam is moved to three different positions with the help of the corrector magnets [27]. At each position, the change in the beam orbit from all BPM readings was recorded after varying the strength of the target quadrupole by a certain ΔK. The orbital changes can be fitted linearly as a function of the beam position in the target quadrupole. An immobile point can be found by setting the position at which the BPM changes vanish. The quadrupole center was then obtained by adding all the immobile points from each BPM. The entire BBA routine repeats this process for all quadrupoles in both the horizontal and vertical planes in the storage ring. To increase the BBA accuracy, the measurement was repeated after moving the beam to the orbit obtained from the previous BBA experiment. This scheme is typically required in the machine commissioning stage. Figure 5 shows the simulated measurements of the horizontal and vertical centers of the quadrupole magnet in the HLS-II storage ring. At least three conventional BBA iterations are required to decrease the standard deviation of the fitted Gaussian function of the quadrupole center to several micrometers, which is of the same order as BPM measurement resolution [28].

3.2 BBA using an NN model

In the simulation, the correctors were set randomly within a certain range of kicks to move the beam orbit. The kick angle variations were generated using a normal distribution with a standard deviation of 0.05 mrad, and a truncation at three standard deviations was applied. For each random orbit, all quadrupoles were simultaneously changed by the same amount of ΔK ($-0.02\,\mathrm{m}^{-2}$). The corresponding initial beam orbit and orbit changes were recorded for all BPMs.

The entire simulation generates 10,000 samples. In each sample, there were 64 initial orbits and 64 orbit change data points, with 32 in the horizontal plane and 32 in the vertical plane. These samples were adopted to train the neural network. Figure 6 shows the random initial beam orbits within the range $(-5, 5)$ mm. Figure 7 shows the orbit change after quadrupole adjustment. The range of the orbit change was within $(-1.5, 1.3)$ mm and $(-0.8, 0.8)$ mm in the horizontal and vertical planes, respectively.

An NN model is trained using these data to obtain the golden orbit. The 64 sets of orbit change data were used as the input to the model, and the 64 sets of the corresponding initial orbit data were used as the output. Eighty percent of the data were used to train the model, and the rest were used to test the performance of the model. There were 128, 256, and 128 neurons in the three hidden layers, respectively. The tanh is considered the activation function that provides nonlinearity. The NN model was trained using the Adam optimizer [29]. The loss function is the mean squared error (MSE) between the measured data and model-predicted results, which is

$$\mathrm{loss} = \mathrm{mean}((\mathbf{r}_{\mathrm{model}} - \mathbf{r}_{\mathrm{real}})^2). \tag{7}$$

Figure 8 compares the golden orbits obtained from the conventional BBA and BBA using a neural network. The consistency between these two BBA methods demonstrates the validity and effectiveness of the new BBA technique. Subsequently, an online experiment was conducted in the HLS-II storage ring.

Table 1 Misalignment error settings used for the HLS-II storage ring

Type axis	Shift error (μm)			Rotation error (μrad)		
	X	Y	S	X	Y	S
Girder	50	50	200	500	500	500
Dipole	200	200	150	500	500	500
Quadrupole	200	200	150	500	500	500
Sextupole	200	200	150	500	500	500
BPM	200	200	150	500	500	500

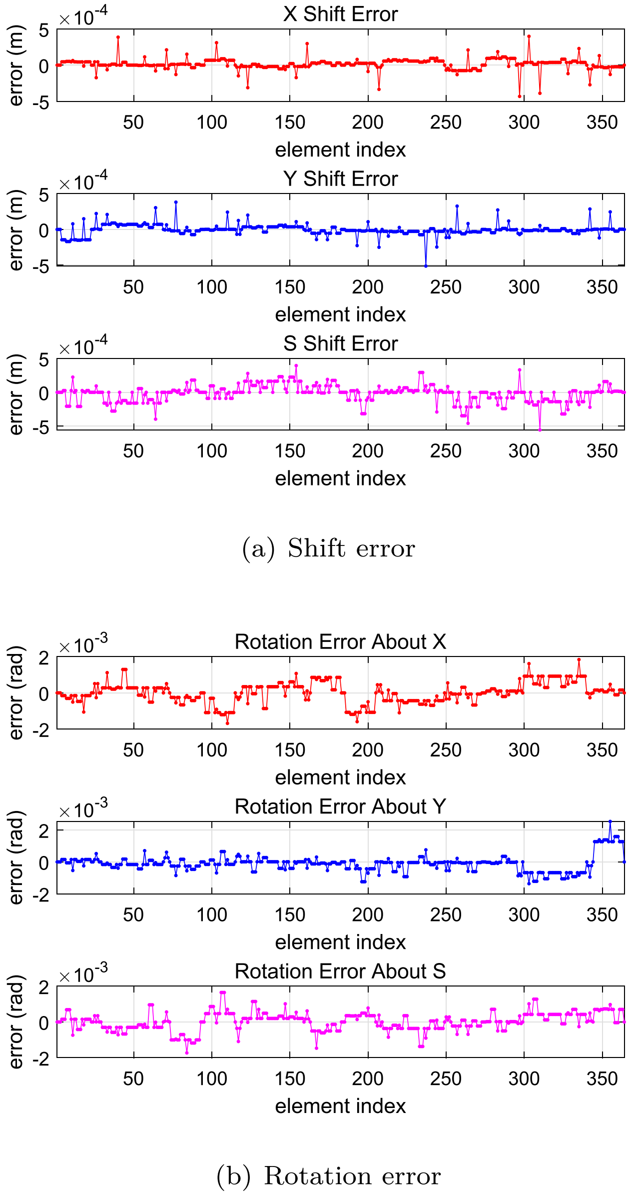

(a) Shift error

(b) Rotation error

Fig. 4 Misalignment errors applied to the HLS-II storage ring. **a** Shift errors. **b** Rotation errors

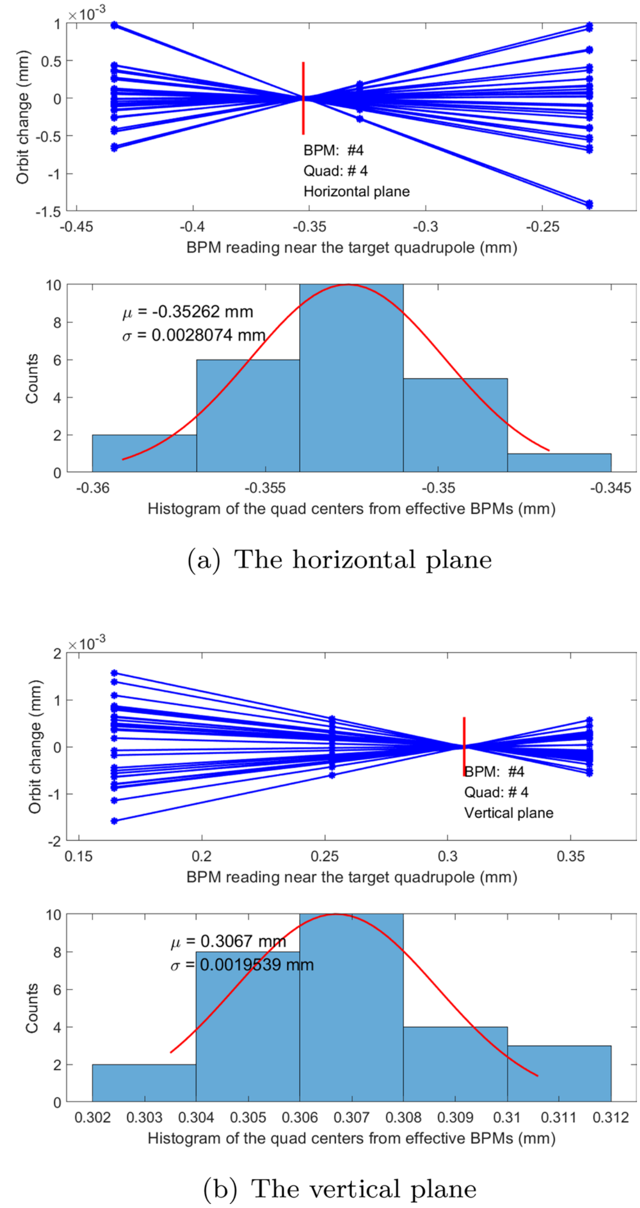

(a) The horizontal plane

(b) The vertical plane

Fig. 5 Simulated BBA measurement in the HLS-II storage ring. The horizontal and vertical measurements are applied, respectively. **a** Horizontal quadrupole center measurement. **b** Vertical qaudrupole center measurement. The plots show the orbit change observed from all BPMs by varying the target quadrupole strength with a certain ΔK when the beam is at three different positions. For each BPM, its changes can be fitted to find a center for the quadrupole. All the found centers are then fitted using the Gaussian function. The red line shows the fitted centers using all BPMs, which represents the BBA center of this quadrupole

4 Online experiment in the HLS-II storage ring

A conventional BBA was applied to the HLS-II storage ring [30]. Figure 9 shows the BBA results for a single quadrupole. The fitting errors for most of the quadrupoles were within 20 μm.

4.1 Training data acquisition

Similar to the simulation, training data can be obtained from a real storage ring. Before the experiment, the magnet strengths were set according to the results of the early commissioning of the storage ring. In this case, the beam is not on the golden orbit that connects the centers of the quadrupoles. An online experiment to obtain the training data is presented in this subsection.

During the online experiment, the orbit feedback system was turned off, and the correctors were randomly

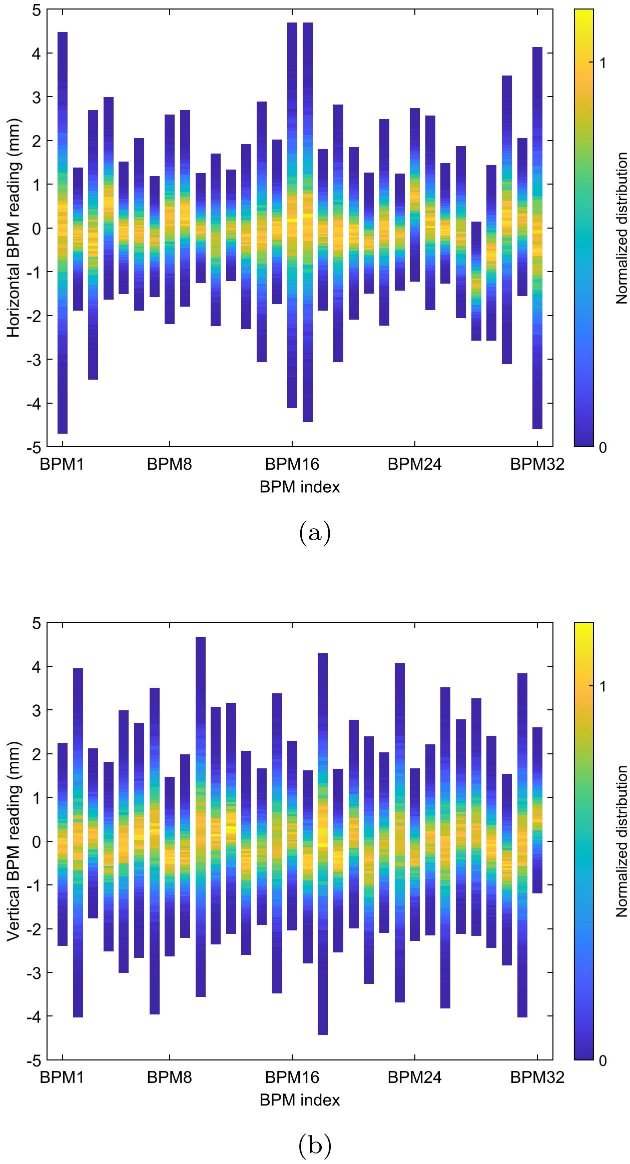

Fig. 6 Distribution of the initial orbits generated by randomly adjusting the orbit correctors within a certain range. **a** Initial orbits in the horizontal plane. **b** Initial orbits in the vertical plane

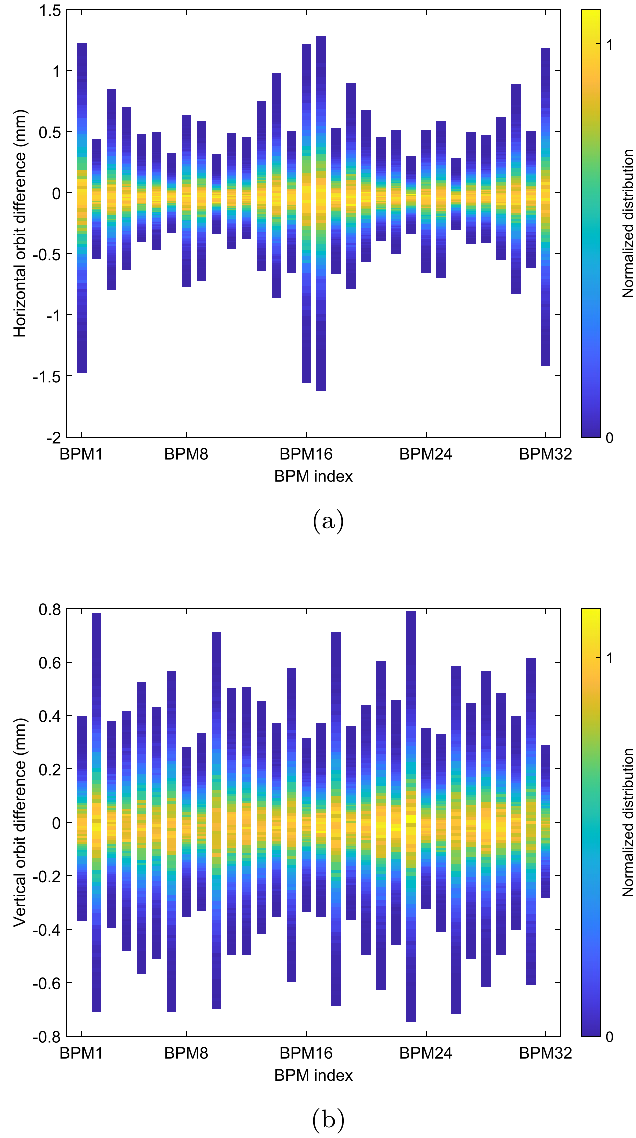

Fig. 7 Distribution of orbit change caused by varying the quadrupole strength for each random orbit in the simulation. **a** Horizontal orbit changes. **b** Vertical orbit changes

set to generate different orbits. As a compromise between beam stability and data diversity, the adjustment range of all correctors was set to ± 0.8A relative to the starting point. This corrector adjustment range ensured no beam loss during the experiment by controlling the orbit change within a distinguishable range, as shown in Fig. 10. The horizontal tune in the HLS-II storage ring was approximately 4.44, whereas the vertical tune was 2.36, which is further from the half-integer. When the quadrupole strength is simultaneously increased, the horizontal tune increases accordingly which may reach the half-integer resonance and thus cause beam loss. Therefore, all quadrupole strengths were adjusted in the decreasing direction by $-0.02\,\mathrm{m}^{-2}$ (normalized focusing strength). After the orbital change was recorded, all quadrupole strengths were restored to their original values. For the HLS-II storage ring, the time constant for the orbit corrector power supply is approximately 15 ms [30]. The time constant for the quadrupole power supply is approximately 30ms. This implies that one complete loop of this measurement could be performed within 1 s. To ensure the data acquisition accuracy, the measurement time for each loop was set to 2 s.

An online experiment was conducted during the machine study time [31]. The entire measurement process generated 21,000 samples. These samples were used to

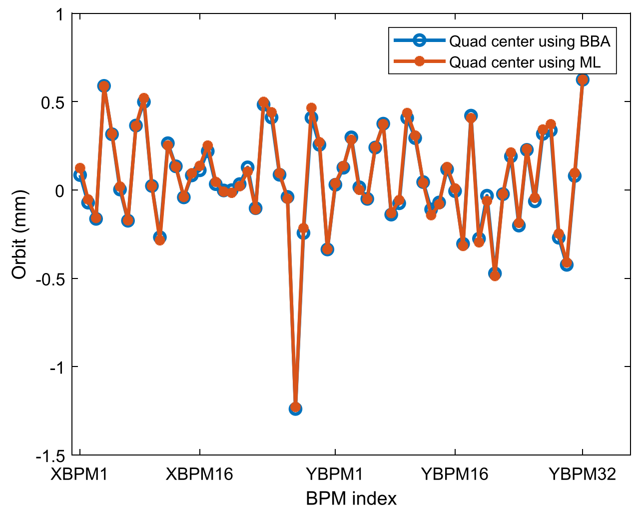

(a) Quadrupole centers

Fig. 8 The quadrupole centers obtained from the conventional BBA and the NN-based BBA. The simulation shows good consistency between these two methods

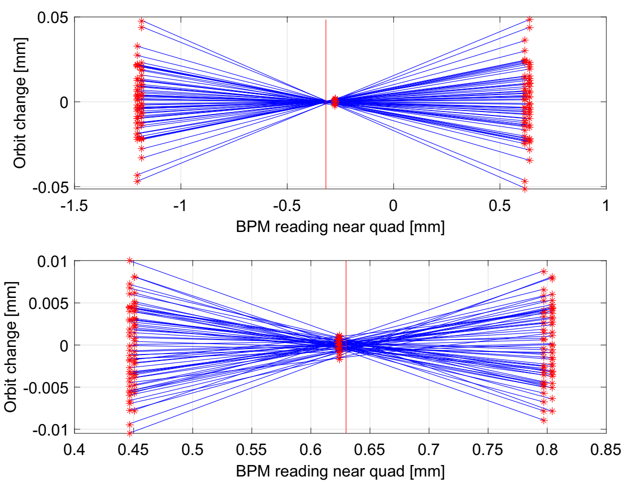

Fig. 9 Measurement of BBA for one quadrupole in the HLS-II storage ring. The upper and lower plots show the horizontal and vertical orbit changes observed from all BPMs by varying the target quadrupole strength with a certain ΔK when the beam is at three different positions. For each BPM, the change in its reading can be fitted to find a center for the quadrupole. The red line shows the averaged fitted centers using all BPMs, which represents the BBA center of this quadrupole

train the neural network. Figure 10 shows the randomly generated initial beam orbits before the quadrupole strength is varied. The distribution shows that orbits were generated within a range of approximately $(-10, 10)$ mm, and the densest distribution was approximately 0. The orbit change after the quadrupole adjustment was also analyzed, and the distribution of the orbit differences

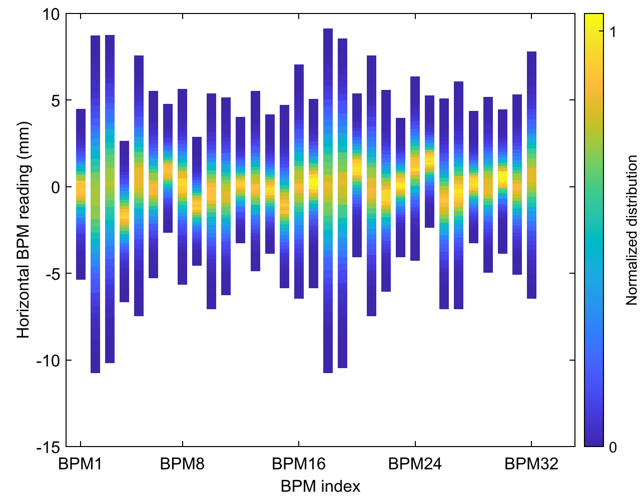

(a)

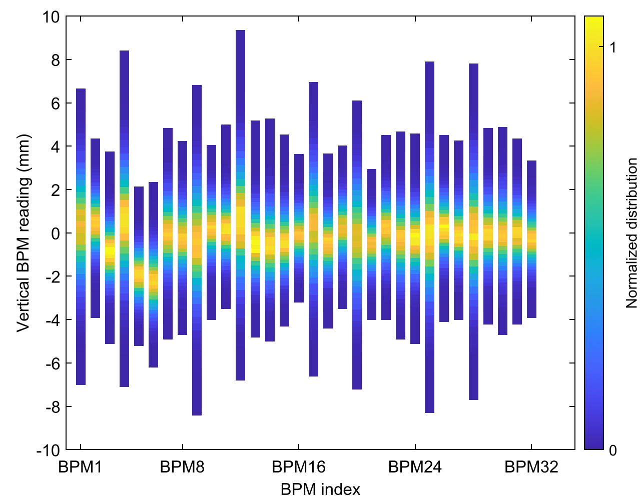

(b)

Fig. 10 Distribution of the orbits generated by randomly adjusting the orbit correctors within a certain range. **a** Horizontal BPM readings. **b** Vertical BPM readings

is plotted in Fig. 11. The range of the orbit change was within $(-3, 2)$ mm in the horizontal plane and within $(-1.5, 1.5)$ mm in the vertical plane.

4.2 NN model training using online data

In this subsection, the relationship between the initial orbit and the orbit change after quadrupole adjustment is explored using a dense neural network. Similar to the simulation, 64 sets of orbit change data were set as the input to the model, and 64 sets of the corresponding initial orbit data were set as the output. To determine the data-size requirements, the two models were trained using different numbers of samples. In

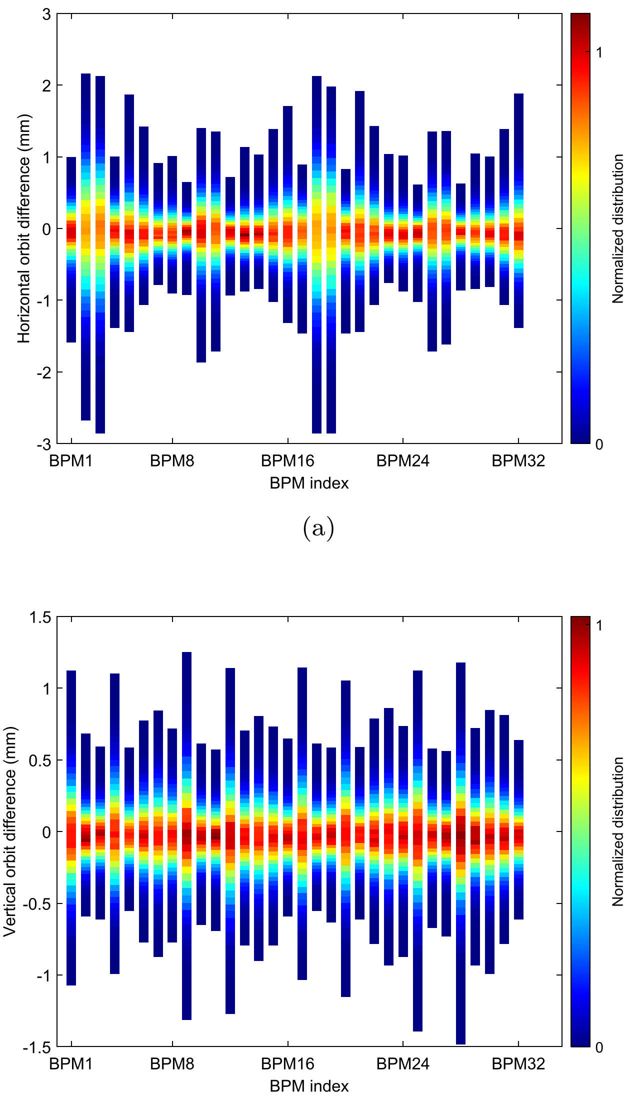

Fig. 11 Distribution of orbit change after varying the quadrupoles for each random orbit. **a** Horizontal orbit change. **b** Vertical orbit change

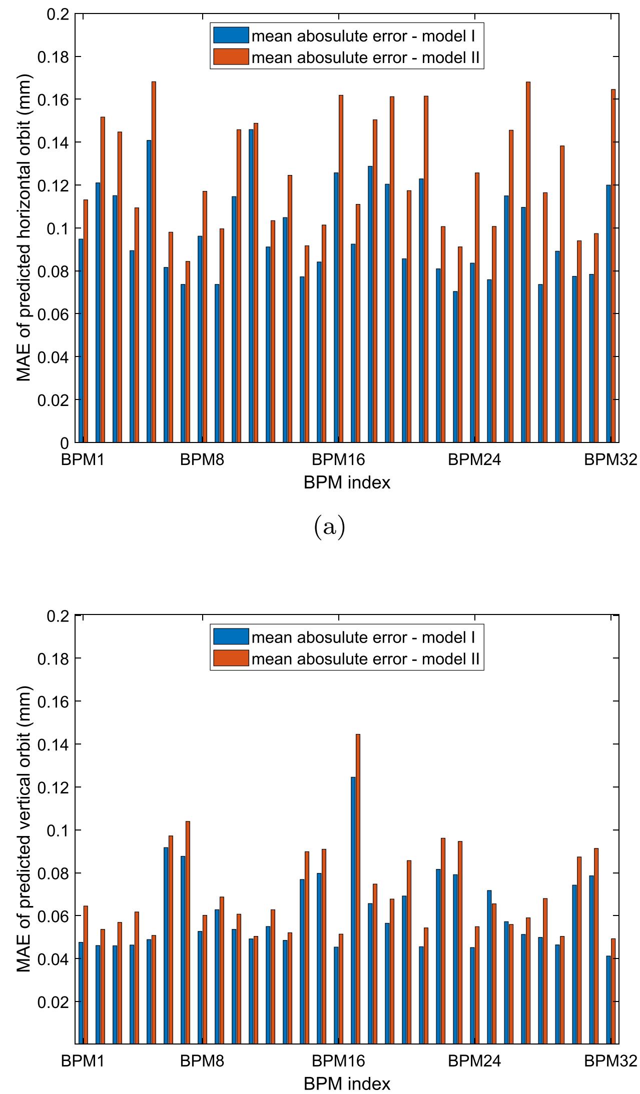

Fig. 12 The mean absolute error (MAE) between the measured beam orbits and predicted values of the validation samples for all BPMs. **a** Horizontal plane. **b** Vertical plane

Model I, all 21,000 samples were adopted, 5/6 of the samples were used for training, and 1/6 were the validation data set. For comparison, Model II was trained with only 3000 samples in the training set and 600 samples in the validation set; 3600 samples were adopted in total. The Adam optimizer and MSE loss function were used to train the models.

The trained NN models were evaluated by calculating the mean absolute error (MAE) between the measured and model-predicted values of the validation samples for each BPM:

$$\mathrm{MAE} = \mathrm{mean}(|\mathbf{r}_{\mathrm{measured}} - \mathbf{r}_{\mathrm{predicted}}|). \tag{8}$$

The absolute errors for both models are shown in Fig. 12, which shows that the errors in model I are smaller than those in model II. In the horizontal plane, the overall average absolute error was approximately 99 μm for Model I and 125 μm for Model II. In the vertical plane, the overall average absolute error was approximately 62 μm for Model I and 71 μm for Model II. The results show that increasing the number of samples for the NN model training can improve the model's accuracy.

4.3 Golden orbit from the NN model

In the NN training, the orbit changes caused by varying quadrupoles were used as the input data. The corresponding initial orbits were used as the output data. The beam on the golden orbit should have the least orbital distortion (ideally zero) owing to the change in quadrupole strength. Therefore, the input can be set to zero for the NN model, and the corresponding output is the golden orbit.

To estimate its accuracy, this golden orbit was compared with that obtained using the conventional BBA method, and the results are shown in Fig. 13. The sub-figures in Fig. 13 illustrate the differences between the novel and conventional BBA. The results show that this golden orbit is consistent with that obtained from the conventional BBA. In the horizontal plane, the average difference between the conventional BBA and the model prediction was approximately 46 µm for Model I and 53 µm for Model II. In the vertical plane, the average difference between the conventional BBA and the model prediction is approximately 42 µm for Model I and 39 µm for Model II.

Although the training error of Model I was smaller than that of Model II, the difference in the predicted golden orbits from these two models did not exhibit a large deviation [32]. In the HLS-II storage ring, the typical experimental period for the conventional BBA process is approximately 5 h. In the machine commissioning phase, this BBA process is needed to be repeated several times to obtain precise results. Model II used only 3600 samples, which resulted in a shorter online measurement time (~ 2 h). As discussed previously, the online measurement time for this new method is irrelevant to the total quadrupole number. This differs from the conventional BBA, where the larger storage ring requires more time. In contrast, the NN-trained golden orbit can be set as the starting point for the conventional BBA. This helps reduce the iterative process of the BBA starting from the initial commissioning orbit and, hence, the experimental time.

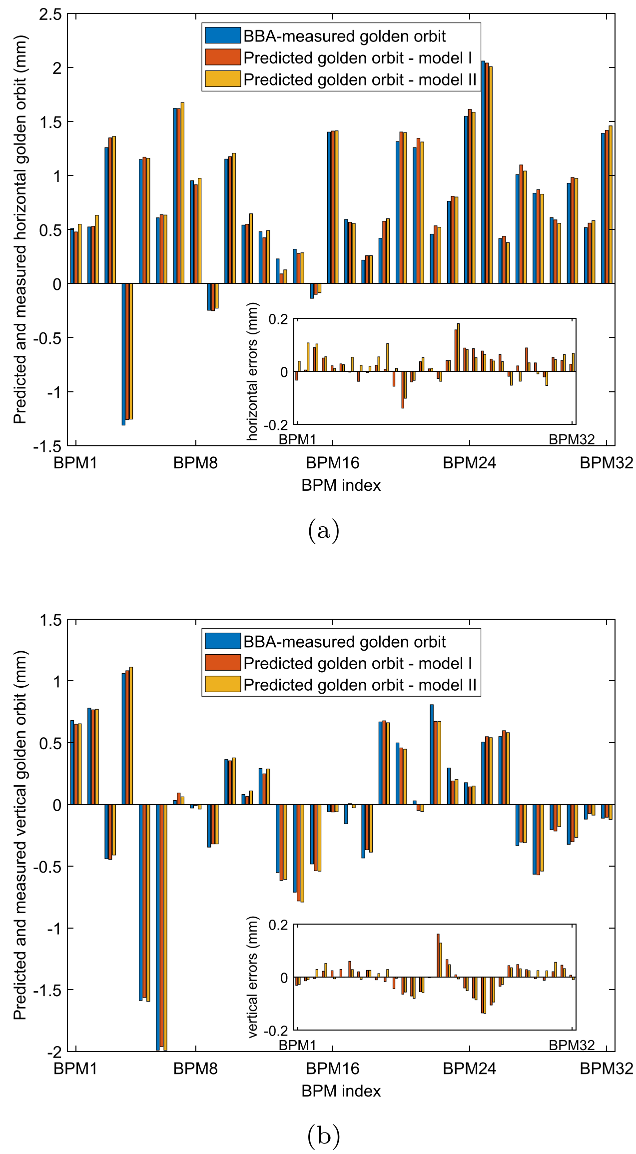

Fig. 13 Comparison of the golden orbit obtained using the NN model and the conventional BBA method. The difference between the two golden orbits is shown in the subfigure. **a** Horizontal golden orbit. **b** Vertical golden orbit

5 Summary

A novel method is developed to search for the golden orbit of a storage ring. This method trains a neural network model using simulated or online data of different closed orbits and the corresponding orbit change caused by simultaneously varying all quadrupole strengths. The online experiments can be conducted in less time, particularly for large storage rings. This golden orbit is compared with that obtained using the conventional BBA, and the result shows good consistency.

The NN-based BBA is a good choice for the commissioning stage of a storage ring, where the beam optics are significantly different from the ideal model and the closed orbit deviates from the magnet centers. In this case, the linear process of conventional BBA is no longer accurate. Moreover, the conventional BBA treats the horizontal and vertical orbits separately. However, the coupling of a real machine is non-negligible, particularly when the coupling is not sufficiently corrected. The NN-based method deals with transverse planes simultaneously, which naturally solves the coupling issue. In addition, the new BBA method can be applied better to storage rings with strong nonlinear effects, which is often the case with DLSRs. With strong nonlinearity, the conventional BBA method might work within a limited region because the linearity of the orbit response is assumed. Because NNs can be used to solve nonlinear problems, as is well known, the NN-based BBA method is expected to be more effective for DLSRs. From another perspective, this new technique can better deal with cases in which the quadrupoles are powered in series, as there is no need to vary the strengths of all quadrupoles individually. Some small light sources or boosters are expected to benefit from the new BBA method.

Acknowledgements The authors thank the engineers and scientists at HLS-II for their valuable suggestions and assistance with the machine studies.

Author Contributions All authors contributed to the study conception and design. Material preparation, data collection and analysis were performed by Guan-Liang Wang, Ke-Min Chen, Si-Wei Wang, and Wei Xu. The first draft of the manuscript was written by Guan-Liang Wang and all authors commented on previous versions of the manuscript. All authors read and approved the final manuscript.

Data Availability Statement The data that support the findings of this study are openly available in Science Data Bank at https://cstr.cn/31253.11.sciencedb.j00186.00488 and https://doi.org/10.57760/sciencedb.j00186.00488.

Declarations

Conflict of interest The authors declare that they have no Conflict of interest.

References

1. X.B. Huang, Simultaneous beam-based alignment measurement for multiple magnets by correcting induced orbit shift. Phys. Rev. Accel. Beams **25**, 052802 (2022). https://doi.org/10.1103/PhysRevAccelBeams.25.052802
2. M. Aiba, M. Böge, H. Braun et al., Study of beam based alignment and orbit feedback for SwissFEL. Proceedings of FEL2010, Malmö, Sweden, 588–591 (2010)
3. A. Madur, P. Brunelle, A. Nadji et al., Beam based alignment for the storage ring multipoles of synchrotron SOLEIL. Proceedings of EPAC 2006, Edinburgh, Scotland. 1939–1941 (2006)
4. Y. Zhao, Y. Jiao, S. Wang, Design study of APS-U-type hybrid-MBA lattice for mid-energy DLSR. Nucl. Sci. Tech. **32**, 71 (2021). https://doi.org/10.1007/s41365-021-00902-1
5. Z. Martí, G. Benedetti, M. Carlà et al., Fast orbit response matrix measurements at ALBA. 8th Int. Particle Accelerator Conf. (IPAC'17), Copenhagen, Denmark, 14 (2017)
6. Z. Martí, G. Benedetti, U. Iriso et al., Fast quadrupole beam based alignment using AC corrector excitations. 9th Int. Particle Accelerator Conf. (IPAC'18), Vancouver, BC, Canada (2018)
7. Z. Martí, G. Benedetti, U. Iriso et al., Fast beam-based alignment using AC excitations. Phys. Rev. Accel. Beams **23**, 012802 (2020). https://doi.org/10.1103/PhysRevAccelBeams.23.012802
8. Z.H. Zhou, Machine learning. Tsinghua University Press, 2016. (in Chinese)
9. A. Edelen, N. Neveu, M. Frey et al., Machine learning for orders of magnitude speedup in multiobjective optimization of particle accelerator systems. Phys. Rev. Accel. Beams **23**, 044601 (2020). https://doi.org/10.1103/PhysRevAccelBeams.23.044601
10. J.Y. Wan, P. Chu, Y. Jiao et al., Improvement of machine learning enhanced genetic algorithm for nonlinear beam dynamics optimization. Nucl. Instrum. Meth. A **946**, 162683 (2019). https://doi.org/10.1016/j.nima.2019.162683
11. J.Y. Wan, P. Chu, Y. Jiao, Neural network-based multiobjective optimization algorithm for nonlinear beam dynamics. Phys. Rev. Accel. Beams **23**, 081601 (2020). https://doi.org/10.1103/PhysRevAccelBeams.23.081601
12. Y.B. Yu, G.F. Liu, W. Xu et al., Research on tune feedback of the Hefei Light Source II based on machine learning. Nucl. Sci. Tech. **33**, 28 (2022). https://doi.org/10.1007/s41365-022-01018-w
13. S.C. Leemann, S. Liu, A. Hexemer et al., Demonstration of machine learning-based model-independent stabilization of source properties in synchrotron light sources. Phys. Rev. Lett. **123**, 194801 (2019). https://doi.org/10.1103/PhysRevLett.123.194801
14. Y.J. Li, W.X. Cheng, L.H. Yu et al., Genetic algorithm enhanced by machine learning in dynamic aperture optimization. Phys. Rev. Accel. Beams **21**, 054601 (2018). https://doi.org/10.1103/PhysRevAccelBeams.21.054601
15. X.Y. Xu, Y.M. Zhou, Y.B. Leng, Machine learning based image processing technology application in bunch longitudinal phase information extraction. Phys. Rev. Accel. Beams **23**, 032805 (2020). https://doi.org/10.1103/PhysRevAccelBeams.23.032805
16. P. Raimondi, N. Carmignani, L.R. Carver et al., Commissioning of the hybrid multibend achromat lattice at the European Synchrotron Radiation Facility. Phys. Rev. Accel. Beams **24**, 110701 (2021). https://doi.org/10.1103/PhysRevAccelBeams.24.110701
17. J. Niedziela, C. Montag, T. Satogata, Quadrupole beam-based alignment at RHIC. Proceedings of the 2005 Particle Accelerator Conference, Knoxville, TN, USA, 2005, pp. 3493–3495. https://doi.org/10.1109/PAC.2005.1591516
18. X.B. Huang, Beam-based correction and optimization for accelerators. CRC Press, 2019. https://doi.org/10.1201/9780429434358
19. S. Grossberg, Nonlinear neural networks: Principles, mechanisms, and architectures. Neural Networks **1**, 17–61 (1988. https://doi.org/10.1016/0893-6080(88)90021-4
20. V.Y. Kreinovich, Nonlinear neural networks: Principles, mechanisms, and architectures. Neural Networks **4**, 381–383 (1991). https://doi.org/10.1016/0893-6080(91)90074-F
21. C.M. Bishop, Neural networks and their applications. Rev. Sci. Instrum. **65**, 1803–1832 (1994). https://doi.org/10.1063/1.1144830
22. A. Terebilo, *Accelerator toolbox for MATLAB*. SLAC National Accelerator Lab, Menlo Park, CA (United States), 2011
23. B. Pang, E. Nijkamp, Y.N. Wu, Deep learning with tensorflow: A review. J. Educ. Behav. Stat. **45**, 227–248 (2020). https://doi.org/10.3102/1076998619872761
24. M. Abadi, A. Agarwal, P. Barham et al., Tensorflow: Large-scale machine learning on heterogeneous distributed systems. arXiv preprint 10.48550/arXiv.1603.04467 (2016).
25. Z.H. Bai, L. Wang, Q.K. Jia et al., Lattice study for the HLS-II storage ring. Chinese Phys. C **37**, 047004 (2013). https://doi.org/10.1088/1674-1137/37/4/047004
26. F.F. Wu, Y.L. Yang, B.G. Sun et al., Introduction of beam position monitor system in the HLS II storage ring. 8th Int. Particle Accelerator Conf. (IPAC'17), Copenhagen, Denmark, 14 (2017)
27. V. Kiselev, V. Smaluk, Measurement of local impedance by an orbit bump method. Nucl. Instrum. Meth. A **525**, 433–438 (2004). https://doi.org/10.1016/j.nima.2004.01.077
28. J.S. Cao, L. M, H.Z. Ma et al., Application of Libera BPM at BEPC II for the early commissioning. Chinese Phys. C **32**, 102–104 (2008)
29. Z.J. Zhang, Improved Adam optimizer for deep neural networks. IEEE/ACM 26th International Symposium on Quality of Service (IWQoS) (2018)
30. W. Xu, J.Y. Li, K. Xuan et al., Orbit stabilization for the HLS-II storage ring. 9th Int. 7th Int. Particle Accelerator Conf. (IPAC'16), Busan, Korea (2016)
31. J.Y. Li, W. Xu, K. Xuan, Operation status of HLS-II. THPOY028, Proceedings of IPAC2016, Busan, Korea, 4155–4158 (2016)

32. G.L. Wang, S.W. Wang, K.M. Chen et al., Beam reference orbit compensation for the HLS-II storage ring. J. Instrum. **18**, T06004 (2023). https://doi.org/10.1088/1748-0221/18/06/T06004